



Article

Rothea serrata Flower Bud Extract Mediated Bio-Friendly Preparation of Silver Nanoparticles: Their Characterizations, Anticancer, and Apoptosis Inducing Ability against Pancreatic Ductal Adenocarcinoma Cell Line

Kariyellappa Nagaraja Shashiraj ¹, Sreenivasa Nayaka ^{1,*}, Raju Suresh Kumar ², Gireesh Babu Kantli ³, Dhanyakumara Shivapoojar Basavarajappa ¹, Pooja Vidyasagar Gunagambhire ¹, Abdulrahman I. Almansour ² and Karthikeyan Perumal ⁴

¹ P. G. Department of Studies in Botany, Karnatak University, Dharwad 580003, Karnataka, India

² Department of Chemistry, College of Science, King Saud University, Riyadh 11451, Saudi Arabia

³ Department of Life Sciences, PIAS, Parul University, Vadodara 391760, Gujarat, India

⁴ Department of Chemistry and Biochemistry, The Ohio State University, 151 W. Woodruff Ave, Columbus, OH 43210, USA

* Correspondence: snayaka@kud.ac.in or sreenivasankud@gmail.com

Abstract: Over past decades, the green method of synthesizing metal nanoparticles has acquired more attentiveness by scientific consensus because of its industrial and biomedical applications. This study focuses on the anti-proliferative effectiveness of AgNPs synthesized from *Rothea serrata* (L.) Steane & Mabb. flower bud extract against the PANC-1 cell line in vitro. Various analytical instruments were utilized to visualize the formation of RsFb-AgNPs, such as UV-Vis spectroscopy, FT-IR, SEM, EDS, TEM, XRD, Zeta potential, and DLS analysis. The biosynthesis of RsFb-AgNPs was observed by a change in color and UV-Vis spectroscopy (415 nm). The FT-IR spectra exhibited the existence of many functional groups. XRD confirmed the crystallinity of the AgNPs. Morphology and elemental mapping were assessed by SEM and EDS analysis. The TEM micrograph revealed spherical-shaped particles with sizes ranging from 12 to 40 nm. Zeta potential and DLS analysis were used to measure surface charge and particle size. Biological properties, including the antioxidant, antimicrobial, and anticancer properties of synthesized RsFb-AgNPs, exhibited dose-dependent activities. In DPPH assay, synthesized RsFb-AgNPs inhibited the scavenging of free radicals in a dose-dependent manner. In addition, the resultant RsFb-AgNPs displayed moderate antimicrobial activity against tested pathogens. Further, the anti-proliferative efficacy of biosynthesized RsFb-AgNPs was determined against the PANC-1 cell line using the MTT assay. The results revealed a dose-dependent decrease in viability of cancer cells with an IC₅₀ value of 36.01 µg/mL. Flow cytometry was then used to confirm the apoptotic effects by double staining with annexin V/PI. In response to the pancreatic ductal adenocarcinoma cell line, the results showed notable early and late apoptosis cell population percentages. In conclusion, the synthesized RsFb-AgNPs revealed a potential anticancer agent that can induce apoptosis in the PANC-1 cells.

Keywords: *Rothea serrata* flower bud; biogenic silver nanoparticles; antioxidant efficacy; anticancer potential; PANC-1 cancer cells; apoptosis



Citation: Shashiraj, K.N.; Nayaka, S.; Kumar, R.S.; Kantli, G.B.; Basavarajappa, D.S.; Gunagambhire, P.V.; Almansour, A.I.; Perumal, K. *Rothea serrata* Flower Bud Extract Mediated Bio-Friendly Preparation of Silver Nanoparticles: Their Characterizations, Anticancer, and Apoptosis Inducing Ability against Pancreatic Ductal Adenocarcinoma Cell Line. *Processes* **2023**, *11*, 893. <https://doi.org/10.3390/pr11030893>

Academic Editors: Ramesa Shafi Bhat and Afaf El-Ansary

Received: 16 February 2023

Revised: 14 March 2023

Accepted: 14 March 2023

Published: 16 March 2023



Copyright: © 2023 by the authors. Licensee MDPI, Basel, Switzerland. This article is an open access article distributed under the terms and conditions of the Creative Commons Attribution (CC BY) license (<https://creativecommons.org/licenses/by/4.0/>).

1. Introduction

Nanotechnology is an interdisciplinary field with advanced avenues in various areas, such as physics, chemistry, biology, and engineering. The primary objective of utilizing nanotechnology is to attain nano-scale particles (1 to 100 nm), also known as nanoparticles (NPs) [1]. Numerous chemical, physical, and biological methodologies exist for synthesizing metallic nanoparticles. Chemical and physical processes are typically expensive, time-consuming, and produce toxic substances that are absorbed on the surface, which

precludes their use in biomedical uses [2,3]. Therefore, a simplistic, adaptable, eco-friendly, empirical, and fiscally feasible approach is necessary for nanoparticle synthesis. Synthesis of NPs using bio-materials such as fungi, bacteria, algae, and plants have been utilized. The use of plants, especially medicinal plants, as a straight forward and efficient biosynthesis process raises researchers' interest based on their biological substance and pharmacological activities [4].

The green synthesis step uses NPs from plant extracts, which has a significant impact on the effectiveness methods, including lower production costs, bio-compatibility, and the potential for trouble-free manufacturing without the use of hazardous chemicals or high temperatures and pressures. Many secondary metabolites are present in plant extracts, and they reduce and stabilize the NPs during their synthesis [5].

Several types of metallic nanoparticles (NPs) have been produced. However, silver nanoparticles (AgNPs) have proven to be the most convenient due to their broad-spectrum applications, such as food, health care, and industry, as well as their unique physical and chemical characteristics [6–8]. The utilization of nanotechnology in the treatment of microbial pathogens, such as fungi and bacteria, has been identified as having considerable potential. They can significantly alter physical, chemical, and biological properties because of their high surface-to-volume ratio [9,10]. Among the many metallic NPs, bio-fabricated AgNPs have exhibited remarkable therapeutic importance, primarily because of their antimicrobial, antioxidant, and anticancer activity against various cancer cells [11–13].

One of the most aggressive cancers in humans is pancreatic ductal adenocarcinoma, with a global 5-year survival rate of less than 9% [14]. Metastatic cancer, known as the most aggressive neoplasm, is a pancreatic cancer. According to previous studies, pancreatic cancer diagnoses increased from 338,000 in 2012 to 458,000 in 2018. Pancreatic cancer claimed the lives of approximately 432,242 people in 2018, and 355,317 new cases are estimated to occur before 2040. This is expected to increase fivefold in the future (GLOBOCAN 2018 estimates) [15,16]. Successful pancreatic cancer diagnosis and treatment are one of the most challenging problems in modern oncology. A vital component of current cancer treatment options, chemotherapy, surgery, immunotherapy, and targeted drugs all have serious negative side effects on cancer patients [17].

As a result, scientists are attempting to develop alternative medications to reduce the number of cancer cases worldwide. Many research communities have developed a diverse variety of NPs using biological methods. Silver nanoparticles significantly impact therapeutic applications because of their anti-diabetic, antioxidant, anticancer, and antimicrobial properties [18]. Plant-mediated AgNPs have shown fascinating selectivity toward malignancy cells in a dose-responsive manner against different malignant tumor cell types, as well as a potentially wide spectrum of anti-proliferative potential. AgNPs synthesized from *Putranjiva roxburghii* seed extract exhibited anticancer activity against MDA-MB 231, PANC-1, and HCT-116 cancer cell lines [19]. *Datura innoxia* flower extract-derived AgNPs had a potential anti-oncogenic activity against the breast cancer (MCF-7) cell line [20], whereas *Delonix regia* extract mediated synthesis AgNPs showed very notable anticancer and therapeutic potential against MCF-7 and Panc-1 cancer cells [21].

Rothea serrata (L.) Steane and Mabb. is a perennial shrub, a small tree, and occasionally a herb that is native to East Asian countries and is a member of the Lamiaceae family. In northern India, it is categorized as being vulnerable. According to the literature, the plant has been used in the folkloric system of medicine since ancient times. Its leaves and roots were used to treat asthma, bronchitis, inflammations, rheumatism, fever, and snakebite [22,23]. The plant is highly medicinal and possesses antioxidant, anticancerous, and neuroprotective properties [24,25]. The usage of the plant's roots and leaves is quite well discussed, whereas the other parts, such as its flowers and buds, have not been comprehensively studied.

Considering the importance of AgNPs synthesis using various plants, to the best of our knowledge, there is no study on *R. serrata* flower bud extract-assisted bio-friendly preparation of AgNPs. Therefore, this research's objective was to synthesize the AgNPs

using an aqueous extract of *R. serrata* flower bud and the in vitro assessment of biological applications.

2. Materials and Methods

2.1. Chemicals

All chemicals and reagents used in experimenting were of AR grade and were purchased from Hi-media Pvt. Ltd. (Mumbai, India) and Loba Chemie Pvt. Ltd. (Mumbai, India). Pathogenic strains, such as *E. coli* (MTCC 40), *P. aeruginosa* (MTCC 9027), *S. aureus* (MTCC 6908), *B. subtilis* (MTCC 6633), *C. albicans* (MTCC 227), and *C. glabrata* (MTCC 3019) were obtained from IMTECH, Chandigarh, India. The PANC-1 cell line was procured from NCCS, Pune, India.

2.2. Collection of Plant Material and Preparation of Flower Bud Extract

Flower buds of *Rothea serrata* were collected from August to October from the outskirts of Hubli-Dharwad (15°44'58.6" N 73°97'27.1" E), followed by a comparison with the herbarium collection of life sciences at the Karnatak University herbarium museum in Dharwad, Karnataka, and the submission of a herbarium voucher number (KU/BOT/2021-22/SN/KNS/Rs-02). The flower buds (Figure 1A,B) were collected and thoroughly washed thrice with tap water and distilled water and then dried in the shade for 10 days. The fine powder was prepared and stored in polythene zip-lock bags using an electric blender. Finely powdered flower buds were approximately weighed (20 g), and minced with 250 mL of Milli-Q water, and the sample was heated at 70 °C for 45 min in a hot water bath. The obtained solution was filtered through Whatman No. 1 filter paper. For further experimental use, the prepared filtrate was stored at 4 °C [26,27].

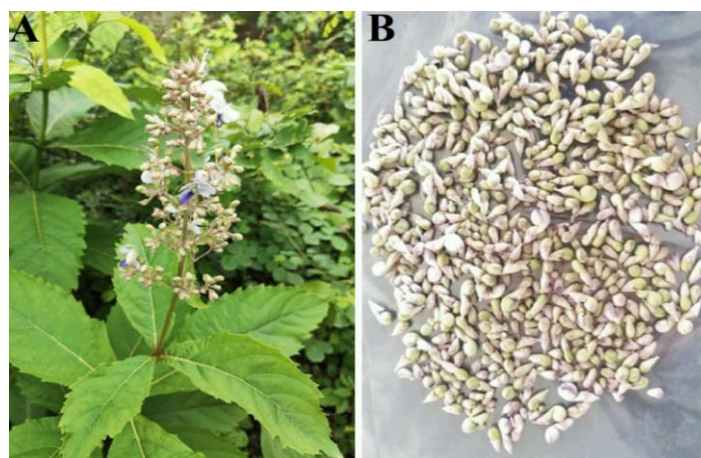


Figure 1. (A) Plant habit of *R. serrata* with flowering twig, and (B) Flower buds.

2.3. Synthesis of AgNPs

For the synthesis of AgNPs, one mM AgNO₃ solution was prepared by mincing 0.169 g in 1 L of distilled water, stored in an amber bottle, and kept in a dark place. In order to optimize the synthesis, the flower bud extract and AgNO₃ solution were added in a ratio of 1:5 (*v/v*) (pH 9.0). The reaction of the suspension was carried out in a dark chamber to avoid photo-activation of AgNO₃. After 24 h, the pale orange color of the solution gradually transformed into dark brownish color as a result of the reduction process. Thus, the color change confirmed that AgNPs had formed. Subsequently, RsFb-AgNPs were obtained by centrifuging the synthesized AgNPs at 12,000 rpm for 15 min. To remove extra biomass, the collected precipitate was centrifuged for 10 min at 12,000 rpm while being re-suspended in 15 mL of Milli-Q water.

The pellet of RsFb-AgNPs was collected with care and dried for 8 h in an oven at 40 °C. The dried powder form of RsFb-AgNPs was stored for further investigation [28].

2.4. Characterizations of Synthesized RsFb-AgNPs

After the synthesis of RsFb-AgNPs, their shape, size, and morphological features were affirmed by various analytical methods. Phyto-fabrication of RsFb-AgNPs was affirmed by UV-Vis. spectrophotometer (METASH UV-9600A, Shanghai, China) in the range of 300 to 600 nm. To ascertain the presence of plant-derived compounds on the biosynthesized RsFb-AgNPs and the *R. serrata* flower bud extract, Fourier Transform Infrared (FTIR) spectroscopy analyses was conducted. Using an FT-IR spectrophotometer instrument (NICOLET 6700, Thermo Fisher Scientific, Waltham, MA, USA), the FTIR spectra of *R. serrata* flower bud extract and RsFb-AgNPs in KBr pellets were measured in the range of 500 to 4000 cm^{-1} . A Cu $K\alpha$ radiation source with an angle of 2θ ranging from 30° to 90° and operating at 40 kV was used to analyze the type of crystallinity of RsFb-AgNPs using an XRD instrument (Rigaku Miniflex 600, Smart-Lab SE, Tokyo, Japan). The topography and elemental details of RsFb-AgNPs were examined by scanning electron microscopy (SEM) linked with an energy dispersive X-ray (EDX) instrument (JEOL, JSM IT 500LA, Peabody, MA, USA) [29]. Transmission electron microscope (TEM) images were acquired to investigate the size and structure of RsFb-AgNPs using (FEI, TECNAI G2, F30, Beijing, China), operated at an acceleration of 300 kV. Prior to analysis, 5 μL of RsFb-AgNPs were placed on the TEM copper grid, followed by the coating with carbon tape and a 48 h drying period in desiccation. Further, to investigate the surface charge and stability in a suspension, RsFb-AgNPs were subjected to zeta potential with DLS analysis to investigate the dispersal pattern size and surface charge of AgNPs with the use of a nano-analyzer instrument (Horiba Scientific SZ-100, Kyoto, Japan) [30,31].

2.5. Antioxidant Potential Analysis by DPPH Assay

The biosynthesized RsLb-AgNPs and *R. serrata* flower bud aqueous extracts were evaluated for their ability to scavenge free radicals using the standard DPPH assay protocol described by Fard et al. [32]. In this study, various concentrations (25–125 $\mu\text{g}/\text{mL}$) of RsFb-AgNPs and *R. serrata* flower bud extract were minced with an equal proportionate volume of 0.1 mM methanolic DPPH solution; ascorbic acid was used as the standard reference. Finally, the reaction mixture was kept at 27°C in the dark for 30 min. The absorbance was measured at 517 nm following the incubation period. A reduction in absorbance hinted at a decrease in DPPH free radicals in the solution; the percentage of inhibition was determined using the below formula.

$$\text{DPPH Scavenging (\%)} = \frac{A_0 - A_1}{A_0} \times 100$$

where A_0 = Absorbance of DPPH and A_1 = Absorbance of the sample

2.6. Antimicrobial Activity of Synthesized RsFb-AgNPs

The antimicrobial activity of synthesized RsFb-AgNPs against selected bacterial and fungal strains was evaluated using the agar well diffusion technique described by Aritonang et al. [33]. For activity testing, we selected two Gram-negative *P. aeruginosa* (MTCC 9027) and *E. coli* (MTCC 40), two Gram-positive *B. subtilis* (MTCC 6633) and *S. aureus* (MTCC 6908), and two fungal strains, *C. glabrata* (MTCC 3019) and *C. albicans* (MTCC 227). Test strains of bacteria and fungi were sub-cultured on their respective broth media. Each culture strain was spread uniformly across the top of nutrient agar plates using sterile cotton swabs. The 6 mm wells on the 4 mm thick agar plates were prepared using a gel-hole puncher. The wells were then loaded with RsLb-AgNPs at 25 to 100 $\mu\text{g}/\mu\text{L}$. The plates were then placed in an incubator and incubated at 37°C for 24 h for bacteria and at 40°C for 72 h for fungi, respectively. Streptomycin and nystatin were used as positive controls. At the end of incubation, the inhibition zone formed around each well was recorded with a transparent ruler in millimeters. To assess the inhibitory activity of synthesized RsFb-AgNPs, MICs were evaluated using the broth micro-dilution protocol in accordance with the CLSI M07 for bacteria, and CLSI M27 for *Candida* sp. The minimal bactericidal concentration (MBC)

and minimal fungicidal concentration (MFC) values of RsFb-AgNPs against four tested bacteria and two *Candida* sp. was examined using a protocol described by Mussin et al. [34].

2.7. *In Vitro* Anticancer Activity of Synthesized RsFb-AgNPs

PANC-1 cells were cultured on Dulbecco's Modified Eagle's Medium (DMEM) under standard conditions and incubated for 24 h at 37 °C in 5% CO₂ atmosphere, 95% humidity, with 10% fetal bovine serum (FBS) added to promote cell proliferation. After incubation, the cells were seeded in 96-well microtiter plates at a density of 20,000 cells/well in 200 µL of complete culture medium. PANC-1 cells were subsequently seeded into wells containing various concentrations of RsFb-AgNPs (12.5–200 µg/mL). After 37 °C, humid incubator incubation at the specified times, cell viability was determined. The assay included doxorubicin (4 µM/mL) as a positive control and cells without RsFb-AgNPs as a negative control. Each well was blended with approximately 200 µL of freshly prepared MTT solution and incubated for 4 h at 37 °C, and a purple color precipitate was observed. After the incubation period, the MTT solution was aspirated from the wells, and 100 µL of buffered DMSO was added to each well to blend the formazan crystals obtained from the study, followed by vigorous shaking of the plates. At a wavelength of 570 nm, viable cells were recorded using a microtiter plate reader (ELX-800, BioTek, Winooski, VT, USA) (Mosmann, 1983; Nagaraja et al., 2022a). The final results were expressed as an IC₅₀ value [35,36].

2.8. Apoptosis Induction Assay by Flow Cytometry

To determine whether PANC-1 cells undergo early apoptosis, late apoptosis, or necrosis following treatment with RsFb-AgNPs, they were stained with annexin V-FITC/PI (Annexin V-FITC apoptosis kit, BD Biosciences, Franklin Lakes, NJ, USA) according to the manufacturer's protocol. Briefly, 6 well plates were seeded with PANC-1 cells (0.5×10^6 cells per well), treated with the IC₅₀ concentration of RsFb-AgNPs (36.01 µg/mL), and incubated at 37 °C in a CO₂ incubator for 24 h. All adhering cells were retrieved with trypsin/EDTA solution, washed two times with PBS buffer solution, and re-suspended with 5 µL of Annexin V/FITC binding buffer for 10 min in the dark prior to incubation at 27 °C. In addition, 5 µL of propidium iodide (PI) and 400 µL of 1X binding buffer were used to stain the cells again for 5 min, and the tubes were gently vortexed. A fluorescence-activated cell sorter (BD FACS Calibur, Flow Cytometer) was then used to analyze the necrotic and apoptotic cell populations in accordance with the standard protocol. BD Cell Quest Pro Ver.6.0 (BD Biosciences) software was used to analyze the obtained experimental data [37].

2.9. Statistical Analysis

All the experiments were performed with three replicates, and the obtained values were represented as mean ± standard error of the mean (SEM). Resultant data were statistically analyzed using SPSS v17 and Origin 2022b version.

3. Results and Discussion

3.1. Synthesis and Characterization of RsFb-AgNPs

In the present study, we synthesized the silver nanoparticles from an aqueous extract of *Rotheca serrata* flower buds. The formation of AgNPs from *R. serrata* flower bud extract was affirmed by the change in color from pale orange to dark brown (Figure 2A–C) after the addition of AgNO₃ (1 mM, at 1:5 ratio), after incubation for 24 h at 27 °C, at pH 9. The change in color from pale orange to dark brown is the initial hint of RsFb-AgNPs formation. The changing of the solution color is due to the excitation of the surface plasmon resonance (SPR) of silver (Ag). UV-Vis spectroscopy is a valuable tool for the visual characterization of AgNPs. The UV-Vis spectra of RsFb-AgNPs exhibit a distinct peak at 415 nm in the range of 300 to 600 nm (Figure 2D), a typical surface plasmon resonance absorption spectrum of the biosynthesized silver nanoparticles. UV-visible spectra also confirmed this; when exposed to light with a wavelength of 400–450 nm, metallic nanoparticles expressed a specific

surface phenomenon known as surface plasmon resonance. As a result, the formation of a distinct peak for silver nanoparticles was revealed by UV-Vis spectroscopic analysis. In general, the absorbance of AgNPs mainly depends on their shape and size [38,39]. Similar outcomes were also reported by Lakshmanan et al. [40], who synthesized AgNPs using fruit extract of *Cleome viscosa*, which displayed surface plasmon resonance absorption peaks between 410 and 450 nm. Rajesh et al. [41] discovered that the plant derived AgNPs from *Couroupita guianensis* Aubl. flower bud extract formed a brownish color when the AgNO_3 was added from the yellow color by adjusting the pH and displayed SPR at 420 nm.

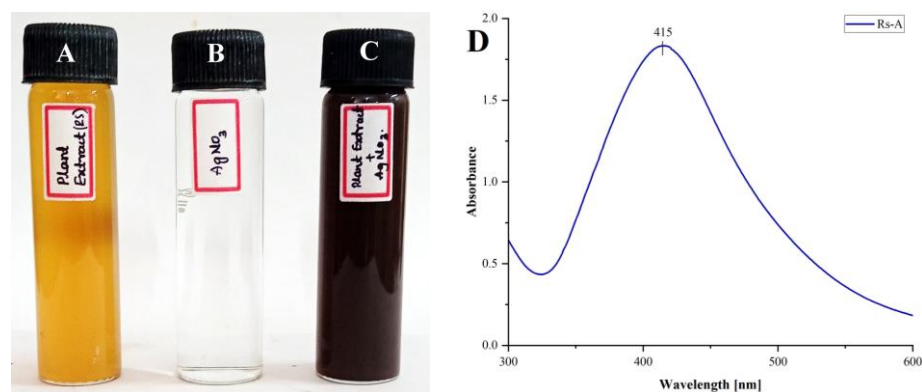


Figure 2. Change in color during the formation of AgNPs. (A) *R. serrata* flower bud extract, (B) silver nitrate solution, (C) reaction mixture (flower bud extract + AgNO_3), and (D) UV-Vis. absorption spectra of RsFb-AgNPs.

3.2. FT-IR Analysis

FT-IR measurements were carried out to quantify and determine the probable functional groups present in the *R. serrata* flower bud extract and synthesized RsFb-AgNPs. Many secondary metabolites were involved in reducing silver ions to silver nanoparticles. Due to the interaction of various functional groups between synthesized materials, there are numerous noticeable peaks in the IR region of the electromagnetic spectrum. The FT-IR spectra of the *R. serrata* flower bud extract exhibited peaks at 582, 812, 1068, 1607, and 3374 cm^{-1} , whereas the RsFb-AgNPs depicted major peaks at 558, 778, 812, 1072, 1384, 1600, 2925, and 3317 cm^{-1} . As a result of the biological reduction process, the FT-IR spectrum of the flower bud extract and the synthesized RsFb-AgNPs displayed very subtle shifts in peak positions. As demonstrated in Figure 3A,B, the FT-IR spectrum of the RsFb-AgNPs differed from the spectra of the flower bud aqueous extract. In AgNPs, FT-IR spectra displayed a peak at 778 cm^{-1} , a weak peak correspond to the (C=C) bending alkene, a medium peak at 1384 cm^{-1} correspond to the (O-H) bending phenol, and a medium sharp peak at 2925 cm^{-1} , corresponding to the (C-H) stretching alkane, those peaks disappeared in the flower bud extract. Both FT-IR spectra showed some typical absorption bands at 582 and 558 cm^{-1} , characteristic of a symmetric vibration of (C-Br) stretching halo compound that was shifted to the lower wave numbers. A similar medium peak in both samples was exhibited at 812 cm^{-1} , representing the (C=C) bending alkene with no shifting in the wave numbers. The vibrational frequency of 1068 and 1072 cm^{-1} assigned to the (C-O) stretching primary alcohol was shifted to the higher wave numbers. Further, the peaks at 1607 and 1600 cm^{-1} correspond to the medium (C=C) stretching cyclic alkene that had shifted lower wave numbers. Finally, 3374 and 3317 cm^{-1} was characteristic of asymmetric vibrational peaks corresponding to the medium (N-H) stretching aliphatic primary amine. The FT-IR spectral analysis of flower bud extract and synthesized RsFb-AgNPs showed the appearance of different functional groups, such as alkanes/alkenes, amines, and alcohol groups, which are responsible for the interaction between biomolecules and metallic nanoparticles. Based on bio-molecules such as carbohydrates, tannins, and flavonoids, phenolic compounds and terpenoids that were present in the flower bud extract have characteristic dual functions that is responsible for the reduction of silver ions to AgNPs [42]. In a previous study, the silver nitrate

was converted to silver nanoparticles using the secondary metabolites found in the extracts, which acts as a stabilizing, reducing, and capping agent [43]. Similarly, Chung et al. [44] described plant extracts as containing various functional groups, such as alkanes, alkenes, amides, and polypeptides, which are meant for capping ionic substances into metallic NPs.

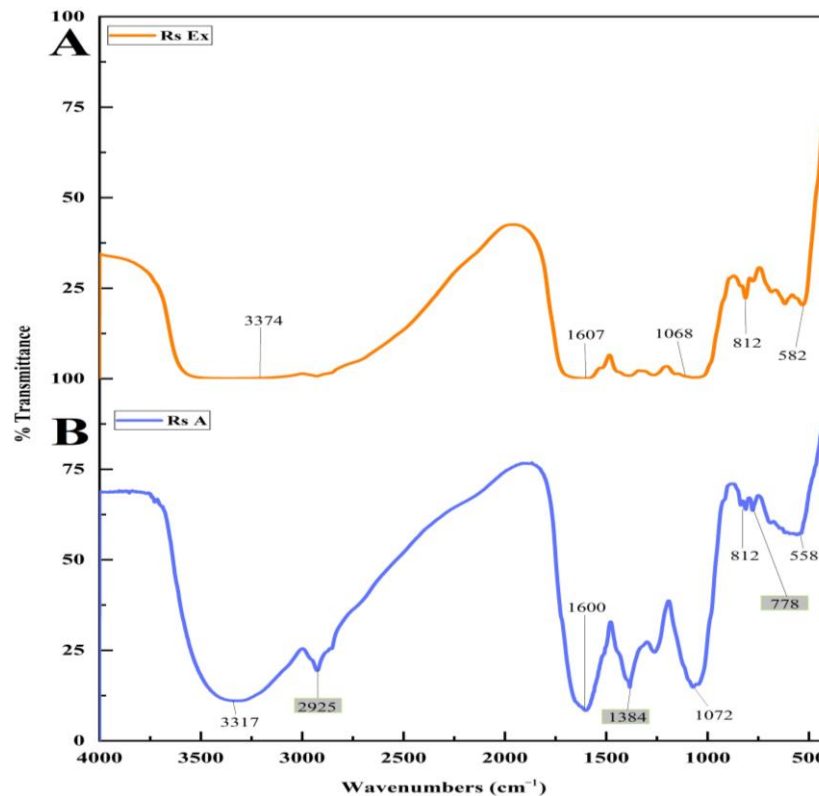


Figure 3. FTIR analysis spectrum of functional groups adsorbed on the surface of (A) flower bud extract and (B) synthesized RsFb-AgNPs.

3.3. XRD Analysis

The crystalline nature of synthesized RsFb-AgNPs was affirmed by XRD analysis. Figure 4 depicts the XRD patterns of RsFb-AgNPs, which displayed four distinct intense diffraction peaks with 2θ values at 38.07° , 44.25° , 64.43° , and 77.30° , which correspond to the lattice reflection planes (111), (200), (220), and (311) of Ag's face-centered cubic (FCC) structure, respectively. The resultant patterns were validated compared to a standard silver card (JCPDS reference code 04-0783). Sharp Bragg's diffraction peaks in the XRD pattern confirmed the synthesis of silver nanoparticles. Due to bio-organic phases on the surfaces of the particle, other unassigned peaks were observed during the XRD analysis [28,36]. A similar outcome of Ajitha et al. [45], in which silver nanoparticles were synthesized using clove (*Syzygium aromaticum*) extract depicted similar diffraction peaks of silver nanoparticles.

3.4. SEM and EDX Analysis

The morphology and topology of the synthesized RsFb-AgNPs were demonstrated via SEM analysis. The obtained RsFb-AgNPs exhibited polydispersed and spherical morphology with agglomeration (Figure 5A). In Figure 5B, the EDX analysis of RsFb-AgNPs reveals a strong signal around 3 and 3.08 keV, indicating the presence of 46.89% of silver due to the discharge of electrons from L and K shells of silver, respectively. A few peaks are attributable to the presence of inorganic impurities in the bio-molecules on the AgNPs surface or chlorine on the glass slide used for the sample preparation process. The carbon peak in the spectral analysis resulted from the carbon adhesive tape used in sample preparation [46]. Arunachalam et al. [47] obtained similar results after they synthesized the

Low zeta potential values of particles suggest neither flocculation nor a tendency for the particles to group due to repulsion forces [50,51]. DLS analysis measures the nanoparticles hydrodynamic size by employing light scattering in an aqueous suspension. In this method, the nanoparticles size and the thickness of a layer of water or bio-molecules absorbed on its surface are measured. The average hydrodynamic particle size distribution RsFb-AgNPs was 95.4 nm (Figure 7B), analyzed by DLS. The significant difference in particle size between TEM size and DLS size is due to the fact that DLS provides hydrodynamic size measurement using aqueous colloidal dispersions and bio-molecules attached to their surfaces, whereas TEM size measurement relies on electron microscopy. In contrast, TEM measurements of particle size after drying only depend on the metallic core of nanoparticles. In addition, determining the average hydrodynamics of a nanoparticle is essential for its biomedical applications as a therapeutic agent [36]. Similarly, Ajitha et al. [52] reported that the surface charges of the nanoparticles predicted the interactions between nanoparticles and the long-term stability of AgNPs in suspension. Higher positive (+30 mV) or higher negative (−30 mV) zeta potential nanoparticles will repel each other and exhibit high stability. El-Aswar et al. [53] reported that the average particle diameter in a previous study was 86.3 nm. The biosynthesized AgNP's zeta potential was discovered as a distinct peak at −42.6 mV.

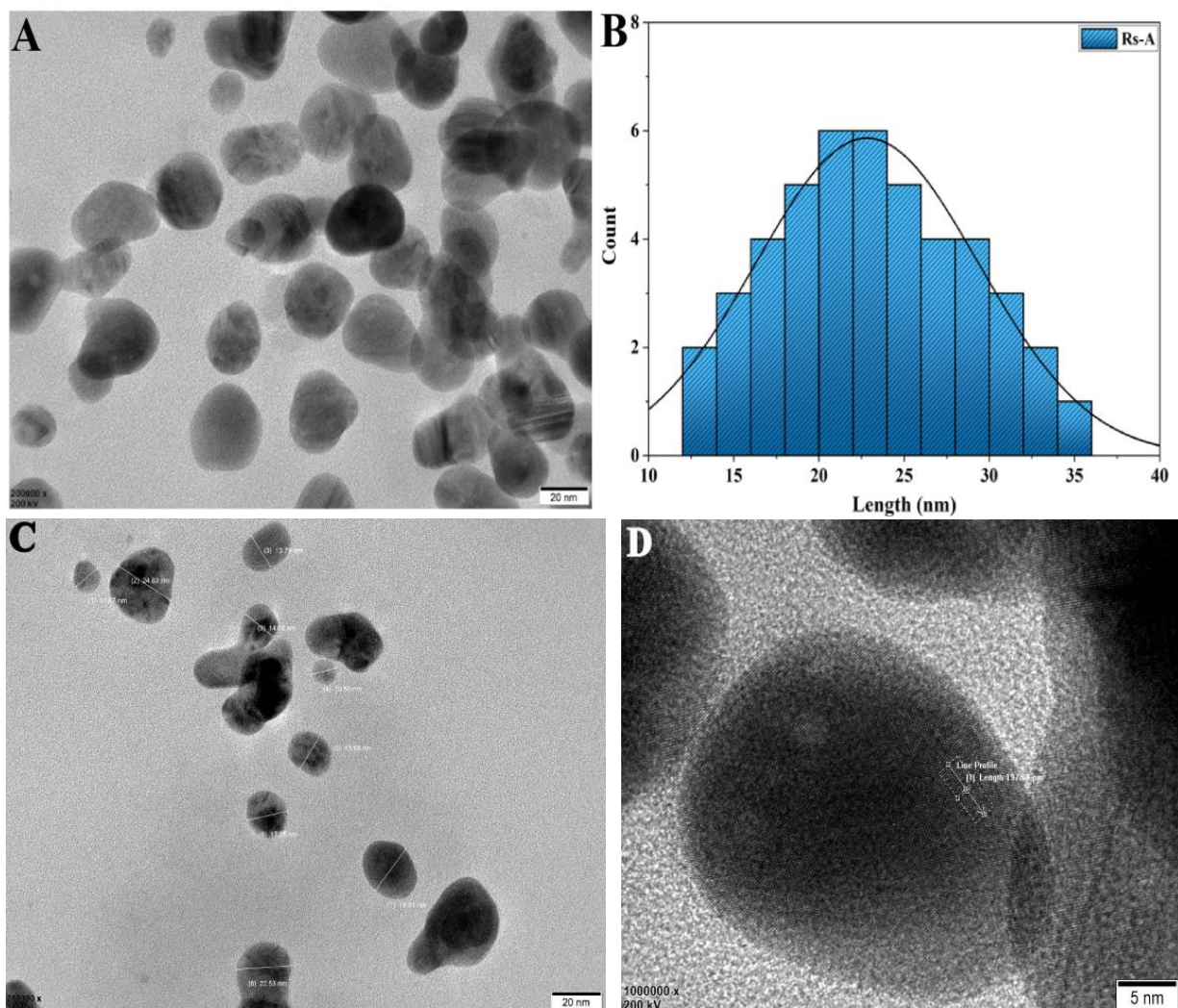


Figure 6. (A) TEM micrograph and (B) histogram of particle size distribution. (C) Selected NPs of the original TEM micrograph for the determination of the size and the shape; (D) d-spacing image showing selected area of lattice fringes.

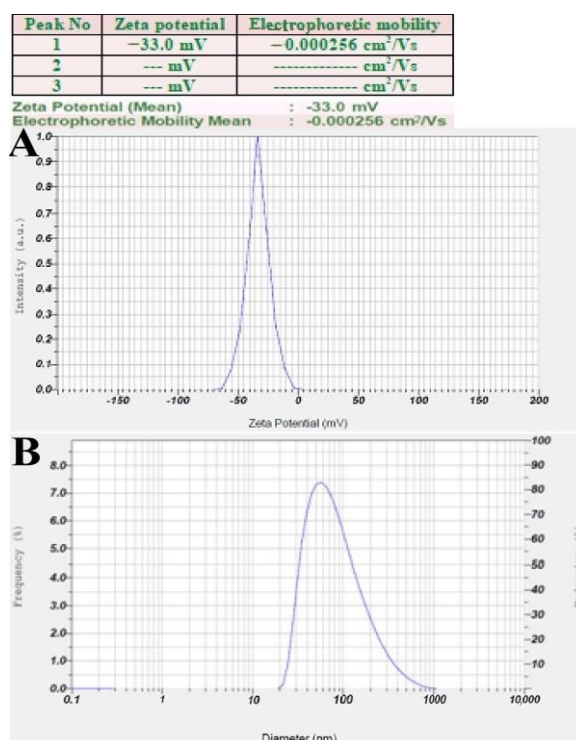


Figure 7. (A) Zeta potential analysis graph. (B) Size intensity analysis graph of synthesized RsFb-AgNPs.

3.7. Antioxidant Activity by DPPH Assay

This study used the DPPH assay to assess the free radical scavenging activity. The DPPH radical scavenging assay is a comparatively quick and reliable method to assess the antioxidant activity of a particular compound. Oxidative activity occurs when molecules are prevented from oxidizing by deterring the oxidative chain reaction's initiation step. This results in the formation of non-reactive stable radicals. The properties of the various phytochemicals present on the surface of synthesized AgNPs mainly determine their antioxidant potential [54–56]. By observing the alteration in color formation, the antioxidant-reducing potentiality of the synthesized AgNPs was ascertained. The RsFb-AgNPs suppressed oxidative stress more effectively than flower bud extract, according to the DPPH assay (Figure 8), with ascorbic acid used as the standard reference, and with an IC₅₀ value of 26.12 µg/mL. In a concentration-dependent way, the RsFb-AgNPs concentration tends to increase the DPPH radical scavenging activity. For flower bud extract, the DPPH activities were 18.3 ± 1%, 29.8 ± 0.2%, 38.2 ± 1, 49.2 ± 0.5, and 63.18 ± 0.2%, with an IC₅₀ value of 76.25 µg/mL, whereas, for RsFb-AgNPs, they were 24.8 ± 0.2%, 39.9 ± 1%, 47.1 ± 0.4%, 57.3 ± 0.2%, and 71.2 ± 1% in the 25, 50, 75, 100, and 125 µg/mL concentration ranges, with an IC₅₀ value of 57.45 µg/mL. These AgNPs have significant anticancer activity, and it takes 36.01 µg/mL to cause 50% cell mortality. In comparison to the flower bud extract, the RsFb-AgNPs showed notable reducing power. As stabilizers and capping agents on the surface of the RsFb-AgNPs, the phenolic compounds in the extract are responsible for this activity. The ability to act as an antioxidant reveals AgNPs' capacity to move electrons and stifle DPPH radicals in the reaction solution [57]. Similar studies have reported on the free radical scavenging activity of AgNPs using extracts of *Lonicera japonica* [58] and *Clerodendrum phlomidis* [59].

3.8. Antimicrobial Activity of RsFb-AgNPs

The antimicrobial activity of biosynthesized RsFb-AgNPs was assessed using the agar well diffusion assay; the inhibition zones were noted as a clear circular zone (mm) on petri plates. Gram-positive, Gram-negative, and fungi were all treated with RsFb-AgNPs. According to the results, *R. serrata* flower bud extract-assisted synthesized AgNPs showed the

maximum growth inhibition for *P. aeruginosa*, *S. aureus*, and *C. albicans*, with inhibition zones recording 19.5 ± 0.9 mm, 18 ± 1.3 mm, and 20.5 ± 1.2 mm, while, *E. coli*, *B. subtilis* and *C. glabrata* showed the least growth inhibition, with zones measuring 18 ± 0.9 mm, 17 ± 1.3 mm, and 17.5 ± 1.2 mm when treated with a 100 μ L concentration of synthesized RsFb-AgNPs. Figure 9 graphically depicts the measured data. Furthermore, the present study's synthesized RsFb-AgNPs significantly inhibited the growth of Gram-positive bacteria. The release of diffusible compounds inhibited by silver nanoparticles causes a zone of inhibition around the well. The composition and thickness of the cell walls may differ, which could explain the variation in the inhibition zones [60,61]. Additionally, by calculating the MIC, MBC, and MFC, the antimicrobial potential of synthesized RsFb-AgNPs against various bacterial and fungal strains was examined. All of the bacterial strains that were tested had values in the range of 6.25 to 50 μ g/mL (Table 1), whereas the fungal strain had values in the range of 50 to 75 μ g/mL (Table 2). The results demonstrate that RsFb-AgNPs were more potent against bacterial strains than against fungal strains, being bactericidal at low concentrations and fungicidal at high concentrations. These differentiations in MBCs and MFCs of the RsFb-AgNPs were due to the distinctness in the cell structure and organization of the bacteria and fungi cells [44,62].

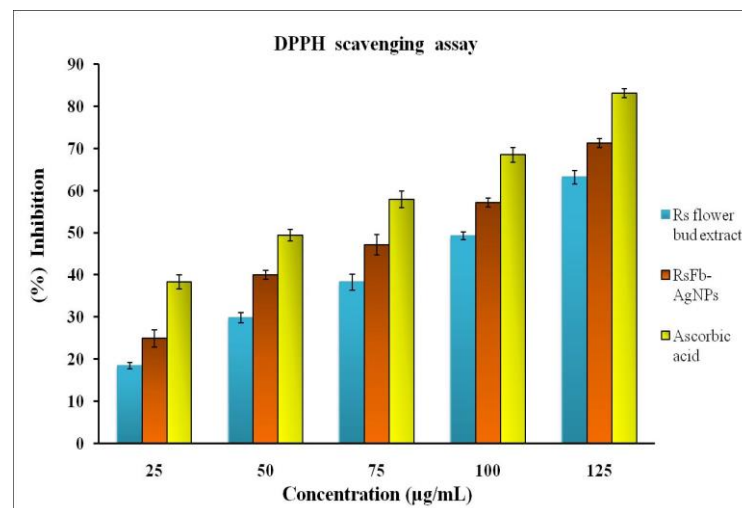


Figure 8. Antioxidant activity of flower bud extract, synthesized RsFb-AgNPs, and standard reference on DPPH radical.

Table 1. MIC and MBC values of synthesized RsFb-AgNPs treated against selected bacterial strains.

Bacterial Strains	MIC (μ g/mL)	MBC (μ g/mL)
<i>S. aureus</i>	6.25	12
<i>B. subtilis</i>	6.25	12
<i>E. coli</i>	12	25
<i>P. aeruginosa</i>	25	50

Table 2. MIC and MFC values of synthesized RsFb-AgNPs treated against selected fungal strains.

Fungal Strains	MIC (μ g/mL)	MFC (μ g/mL)
<i>C. albicans</i>	25	75
<i>C. glabrata</i>	12.5	50

According to studies, synthesized RsFb-AgNPs may interact with and disrupt the bacterial membrane surface, increasing cell permeability and inhibiting or changing cellular respiration. As a result, it causes enzymes to degrade, disrupts DNA proteins, and ultimately results in the death of these cells [63]. Another potential consequence of the

antimicrobial properties of AgNPs is the release of silver ions from them, which may bind to oxygen, sulfur, and nitrogen in the functional bio-molecules of bacterial cells and cause their death [64]. Similarly, in comparison to earlier reports where AgNPs were synthesized from *Argyria nervosa* extract, Gram-positive bacteria were found to be less susceptible than Gram-negative ANE-AgNPs. Increasing ANE-AgNPs concentration increased the zone of inhibition formed [65]. In a previous study, Lee et al. [66] revealed that *T. farfara* flower bud extract-derived Tf-AgNPs exhibited significantly inhibition to the growth of the tested microorganisms.

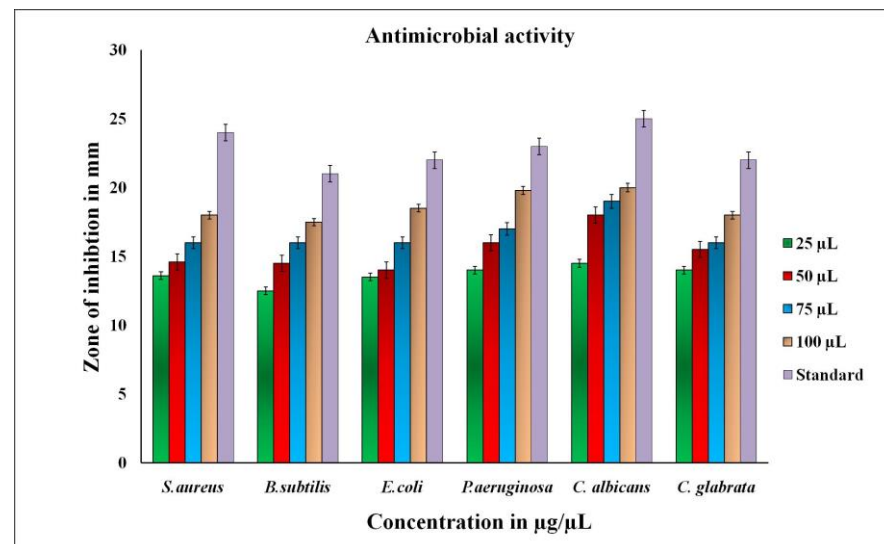


Figure 9. Graphical representation of antimicrobial activity showing the zone of inhibition to synthesized RsFb-AgNPs, and standard reference against tested microorganisms.

In a previous study, MIC and MBC values of *Murraya koenigii* (L.) green synthesized AgNPs (13–14 mm) on *Escherichia coli* was reported as 16 µg/mL and 32 µg/mL, respectively, while for *S. aureus* the MICs and MBCs values were 32 µg/mL and 64 µg/mL [67]. Furthermore, 62 µg/mL and 125 µg/mL MICs and MFCs values of biosynthesized AgNPs (13 mm) against *Candida* sp. was published by Jalal et al. [68].

3.9. In Vitro Anticancer Activity of RsFb-AgNPs

The colorimetric MTT assay was used to assess the in vitro cytotoxic potential of RsFb-AgNPs against PANC-1 (pancreatic ductal adenocarcinoma) cells at various concentrations of RsFb-AgNPs. The results were measured in absorbance at 570 nm because this assay is a colorimetric measurement. In Figure 10A–G, the cell treated with RsFb-AgNPs shows morphological changes. These AgNPs have significant anticancer activity, and it takes 36.01 µg/mL to cause 50% cell mortality. At 12.5, 25, 50, and 100 µg/mL of RsFb-AgNPs, respectively, a dose-dependent decrease in the percentage of cell viability was measured to be 75.6%, 63.6%, 42.5%, and 20.2%, and it was decreased to 3.32% when served with 200 µg/mL of RsFb-AgNPs. These percentages are graphically shown in Figure 10H. AgNPs' inhibitory mechanism for cancer cell lines is not well understood. However, it was hypothesized that AgNPs could inhibit the activity of abnormally increased signaling proteins or interacts with functional groups of intracellular proteins and enzymes and the nitrogen bases in DNA, which would cause cell death [63]. Similar results were demonstrated by Shameli et al. [21], who found that the anti-oncogenic potential of *D. regia* mediated silver nanoparticles was enhanced by increasing the AgNPs concentrations and decreasing the cell viability percentages against Panc-1 cancer cells over time. Another report by Kanniah et al. [69] showed that silver-based chitosan nanoparticles mediated

by *P. nigrum* seed extract showed inhibition of the cell viability of the pancreatic ductal adenocarcinoma cell lines at concentrations differing from 10 to 200 $\mu\text{g}/\text{mL}$.

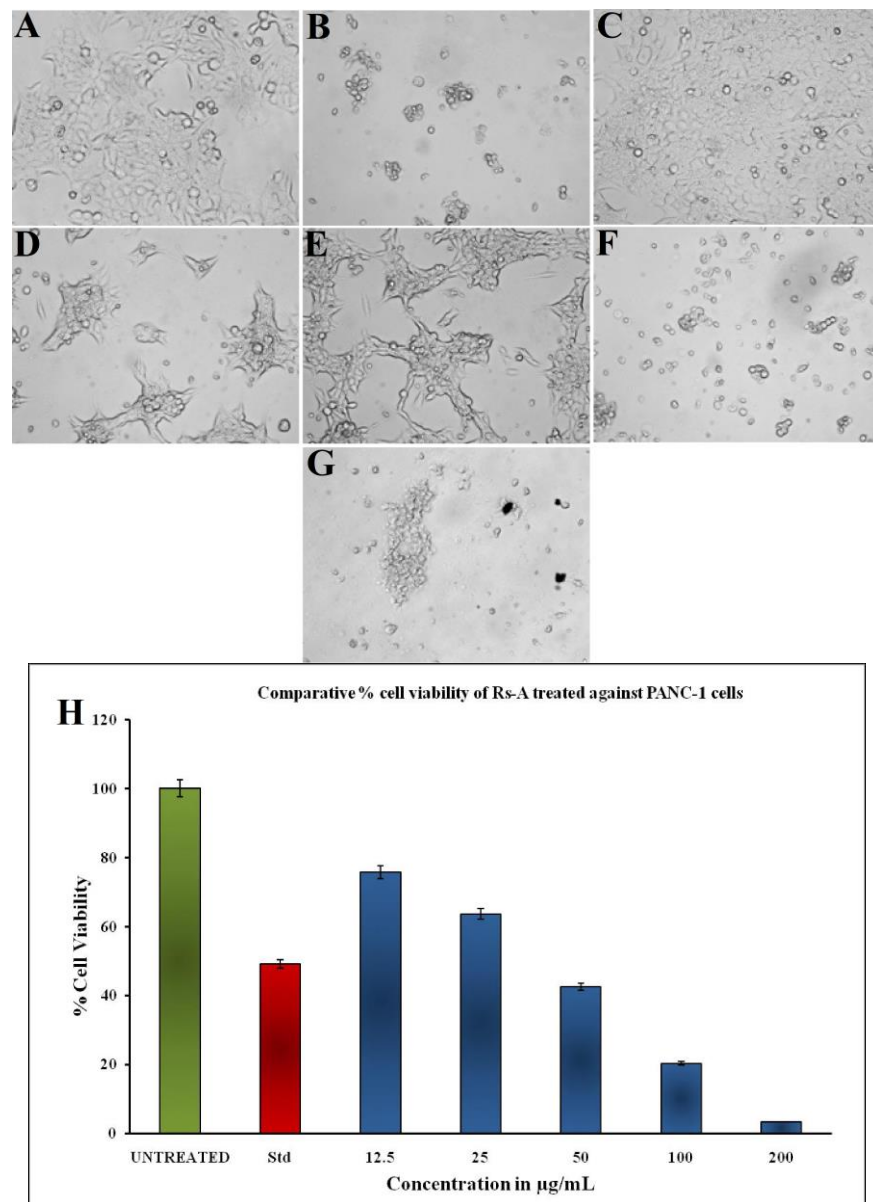


Figure 10. Cell viability of PANC-1 cells treated with synthesized RsFb-AgNPs: (A) Negative control, (B) Positive control, (C) 12.5 $\mu\text{g}/\text{mL}$, (D) 25 $\mu\text{g}/\text{mL}$, (E) 50 $\mu\text{g}/\text{mL}$, (F) 100 $\mu\text{g}/\text{mL}$, and (G) 200 $\mu\text{g}/\text{mL}$. (H) Bar graph showing the comparative percentage of cell viability.

3.10. Apoptotic Induction Studies

The annexin V-mediated apoptosis of PANC-1 cells was examined by staining the cells with annexin V/PI, followed by flow cytometry detection, to determine whether an apoptotic pathway induces the cytotoxicity caused by RsFb-AgNPs. The results are depicted in Figure 11A for untreated cells and in Figure 11B for treated cells. The quadrant plots exhibit the patterns of how silver nanoparticles affect PANC-1 cancer cells ability to survive, with the quadrant lower left (Q1) representing the percentage of viable cells (33.02%), the quadrant upper left (Q2) depicting the percentage of dead cells (3.20%), the quadrant upper right (Q3) expressing the percentage of late apoptotic cells (55.32%), and the quadrant (Q4) lower right showing the % of early apoptotic cells (8.46%). The results were measured after a 24 h treatment with RsFb-AgNPs at an IC_{50} concentration of 36.01 $\mu\text{g}/\text{mL}$.

Figure 11C,D displays the cell cycle analysis using the markers M1 and M2. The untreated cells expressed 0.28% of M2 and 99.72% of M1 viable cells (Figure 11C). M1 corresponded to 19.81% of the viable PANC-1 cancer cells, whereas M2 represents 80.19% of the damaged cells (Figure 11D). In contrast to untreated cells, which showed no significant apoptosis, treated cells demonstrated significant early and late apoptosis cell populations against Panc-1 cells. The % of early and late apoptosis in the treated cell line is indicated by the obtained results, which showed the apoptotic effect of the synthesized RsFb-AgNPs. The obtained results were in comparison with the standard used against PANC-1 cells and showed apoptotic rates of 35.05% for viable cells, 0.32% for dead cells, 42.29% for late apoptotic cells, and 22.34% for early apoptotic cells. The apoptotic rate percentages are graphically depicted in Figure 11E. Similarly, Fard et al. [32] reported that when A549 cancer cells were treated with 10.3 $\mu\text{g}/\text{mL}$ AgNPs, the synthesized silver nanoparticles displayed 53.67% of late apoptosis and 7.70% of early apoptosis. Another study by Nagaraja et al. (2022b) reported that the *Cucumis sativus* var. *hardwickii* fruit extract-mediated AgNPs exhibited 57% induced apoptosis against Pa-1 cancer cells [70].

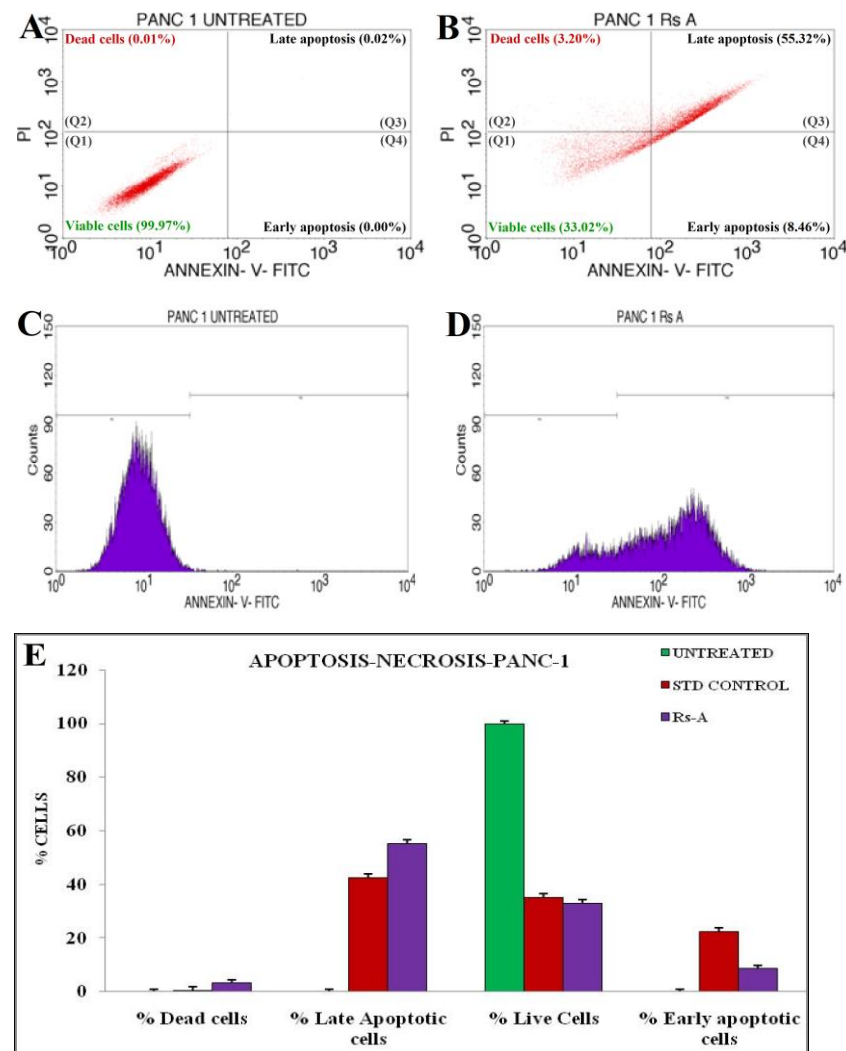


Figure 11. Quadrangular plots showing the flow cytometric cell viability test of PANC-1 cells after treatment with an IC_{50} concentration of synthesized RsFb-AgNPs: (A) untreated, (B) treated cells with an IC_{50} concentration of synthesized RsFb-AgNPs, (C) cell cycle analysis of untreated control sample, and (D) treated cells with an IC_{50} concentration of synthesized RsFb-AgNPs. (E) Graph showing the comparative percentage of apoptotic rate in standard drug, untreated, and treated cells.

4. Conclusions

To summarize, a sustainable biogenic method was employed to synthesize silver nanoparticles using *R. serrata* flower bud extract, which revealed polydispersed, spherical-shaped RsFb-AgNPs. The phyto-molecules in the extracts served as safe reducing, stabilizing, and capping agents that could turn silver ions into silver nanoparticles. A different set of analytical methods was used to examine biosynthesized RsFb-AgNPs, and the results confirmed the formation of the NPs as well as their shape, size, crystallinity, and surface charge. Additionally, antioxidant, antimicrobial, and anti-proliferative tests were used to evaluate the potency of phyto-fabricated RsFb-AgNPs. The RsFb-AgNPs demonstrated good antimicrobial activity against the tested microorganisms and significantly reduced the DPPH free radicals in a dose-dependent manner. Further, to ascertain the percentage of cell viability, the biosynthesized RsFb-AgNPs were tested for cytotoxicity against the PANC-1 cell line using the MTT assay. The synthesized RsFb-AgNPs exhibited a gradual decrease in % of cell viability with the increase in concentration. The consequent IC₅₀ value was found to be 36.01 µg/mL. In addition, apoptotic studies were conducted using the flow cytometry technique. The PANC-1 cell line displayed significant early and late apoptosis by showing 8.46 % and 55.32% of the cell population. Hence, the promising potential shown by *R. serrata* flower bud extract-assisted AgNPs in vitro studies highlights that AgNPs can be scaled up to investigate various biomedical applications.

Author Contributions: Conceptualization, S.N. and K.N.S.; methodology, K.N.S.; software, R.S.K.; validation, R.S.K., A.I.A. and K.P.; investigation, K.N.S.; data curation, G.B.K.; writing—original draft preparation, K.N.S.; writing—review and editing, K.N.S. and S.N.; visualization, D.S.B. and P.V.G.; supervision, S.N. All authors have read and agreed to the published version of the manuscript.

Funding: This project was funded by the Researchers Supporting Project number (RSP2023R142), King Saud University, Riyadh, Saudi Arabia.

Institutional Review Board Statement: Not applicable.

Informed Consent Statement: Not applicable.

Data Availability Statement: All data generated or analyzed during this study are included in this published manuscript.

Acknowledgments: The authors are thankful to the P. G. Department of Studies in Botany for providing the laboratory facility and to Sophisticated Analytical Instrumentation Facility (SAIF), University Scientific Instrumentation Centre (USIC), Karnatak University Dharwad for extending necessary instrumentation facilities, and Backward Classes Welfare Department, Government of Karnataka for the financial support in the form of a fellowship to one of the author (K.N.S).

Conflicts of Interest: The authors declare no conflict of interest.

References

1. Khandel, P.; Yadaw, R.K.; Soni, D.K.; Kanwar, L.; Shahi, S.K. Biogenesis of metal nanoparticles and their pharmacological applications: Present status and application prospects. *J. Nanostruct. Chem.* **2018**, *8*, 217–254. [[CrossRef](#)]
2. Guo, T.; Yao, M.S.; Lin, Y.H.; Nan, C.W. A comprehensive review on synthesis methods for transition-metal oxide nanostructures. *CrystEngComm* **2015**, *17*, 3551–3585. [[CrossRef](#)]
3. Das, P.; Ghosal, K.; Jana, N.K.; Mukherjee, A.; Basak, P. Green synthesis and characterization of silver nanoparticles using belladonna mother tincture and its efficacy as a potential antibacterial and anti-inflammatory agent. *Mat. Chem. Phys.* **2019**, *228*, 310–317. [[CrossRef](#)]
4. Makarov, V.V.; Love, A.J.; Sinitsyna, O.V.; Makarova, S.S.; Yaminsky, I.V.; Taliany, M.E.; Kalinina, N.O. Green nanotechnologies: Synthesis of metal nanoparticles using plants. *Acta Nat.* **2014**, *6*, 35–44. [[CrossRef](#)]
5. Gudikandula, K.; Charya Maringanti, S. Synthesis of silver nanoparticles by chemical and biological methods and their antimicrobial properties. *J. Exp. Nanosci.* **2016**, *11*, 714–721. [[CrossRef](#)]
6. Sekhon, B. Nanotechnology in agri-food production: An overview. *Nanotechnol. Sci. Appl.* **2014**, *7*, 31–53. [[CrossRef](#)] [[PubMed](#)]
7. Thiruvengadam, M.; Rajakumar, G.; Chung, I.M. Nanotechnology: Current uses and future applications in the food industry. *3 Biotech* **2018**, *8*, 74. [[CrossRef](#)]

8. Rehman, S.; Jermy, R.; Mousa Asiri, S.; Shah, M.A.; Farooq, R.; Ravinayagam, V.; Azam Ansari, M.; Alsalem, Z.; Al Jindan, R.; Reshi, Z.; et al. Using *Fomitopsis pinicola* for bioinspired synthesis of titanium dioxide and silver nanoparticles, targeting biomedical applications. *RSC Adv.* **2020**, *10*, 32137–32147. [[CrossRef](#)] [[PubMed](#)]
9. Nayak, S.; Bhat, M.P.; Udayashankar, A.C.; Lakshmeesha, T.R.; Geetha, N.; Jogaiah, S. Biosynthesis and characterization of *Dillenia indica*-mediated silver nanoparticles and their biological activity. *Appl. Organometal. Chem.* **2020**, *34*, e5567. [[CrossRef](#)]
10. Kim, S.W.; Jung, J.H.; Lamsal, K.; Kim, Y.S.; Min, J.S.; Lee, Y.S. Antifungal effects of silver nanoparticles (AgNPs) against various plant pathogenic fungi. *Mycobiology* **2012**, *40*, 53–58. [[CrossRef](#)] [[PubMed](#)]
11. Mohamed, Y.M.A.; Elshahawy, I.E. Antifungal activity of photo-biosynthesized silver nanoparticles (AgNPs) from organic constituents in orange peel extract against phytopathogenic *Macrophomina phaseolina*. *Eur. J. Plant. Pathol.* **2022**, *162*, 725–738. [[CrossRef](#)]
12. Basavarajappa, D.S.; Kumar, R.S.; Almansour, A.I.; Chakraborty, B.; Bhat, M.P.; Nagaraja, S.K.; Hiremath, H.; Perumal, K.; Nayaka, S. Biofunctionalized silver nanoparticles synthesized from *Passiflora vitifolia* leaf extract and evaluation of its antimicrobial, antioxidant and anticancer activities. *Biochem. Eng. J.* **2022**, *187*, 108517. [[CrossRef](#)]
13. Burduşel, A.C.; Gherasim, O.; Grumezescu, A.M.; Mogoanta, L.; Ficai, A.; Andronesu, E. Biomedical applications of silver nanoparticles: An up-to-date overview. *Nanomaterials* **2018**, *8*, 681. [[CrossRef](#)] [[PubMed](#)]
14. Yang, S.; Kimmelman, A.C. A critical role for autophagy in pancreatic cancer. *Autophagy* **2011**, *7*, 912–913. [[CrossRef](#)]
15. Bray, F.; Ferlay, J.; Soerjomataram, I.; Siegel, R.L.; Torre, L.A.; Jemal, A. Global Cancer Statistics 2018: GLOBOCAN estimates of incidence and mortality worldwide for 36 cancers in 185 countries. *CA Cancer J. Clin.* **2018**, *68*, 394–424. [[CrossRef](#)] [[PubMed](#)]
16. Siegel, R.L.; Miller, K.D.; Jemal, A. Cancer Statistics, 2018. *CA Cancer J. Clin.* **2018**, *68*, 7–30. [[CrossRef](#)]
17. Patra, J.K.; Das, G.; Fraceto, L.F.; Campos, E.V.R.; del Rodriguez-Torres, M.P.; Acosta-Torres, L.S.; Diaz-Torres, L.A.; Grillo, R.; Swamy, M.K.; Sharma, S.; et al. Nano based drug delivery systems: Recent developments and future prospects. *J. Nanobiotechnol.* **2018**, *16*, 71. [[CrossRef](#)]
18. Yang, F.; Jin, C.; Jiang, Y.; Li, J.; Di, Y.; Ni, Q.; Fu, D. Liposome based delivery systems in pancreatic cancer treatment: From bench to bedside. *Cancer. Treat. Rev.* **2011**, *37*, 633–642. [[CrossRef](#)] [[PubMed](#)]
19. Balkrishna, A.; Sharma, V.K.; Das, S.K.; Mishra, N.; Bisht, L.; Joshi, A.; Sharma, N. Characterization and anti-cancerous effect of *Putranjiva roxburghii* seed extract mediated silver nanoparticles on human colon (HCT-116), pancreatic (PANC-1) and breast (MDA-MB 231) cancer cell lines: A comparative study. *Int. J. Nanomed.* **2020**, *15*, 573–585. [[CrossRef](#)]
20. Gajendran, B.; Durai, P.; Varier, K.M.; Liu, W.; Li, Y.; Rajendran, S.; Nagarathnam, R.; Chinnasamy, A. Green synthesis of silver nanoparticle from *Datura innoxia* flower extract and its cytotoxic activity. *BioNanoScience* **2019**, *9*, 564–572. [[CrossRef](#)]
21. Shameli Rajiri, M.; Aminsalehi, M.; Shahbandeh, M.; Maleki, A.; Jonoubi, P.; Rad, A.C. Anticancer and therapeutic potential of *Delonix regia* extract and silver nanoparticles (AgNPs) against pancreatic (Panc-1) and breast (MCF-7) cancer cell. *Toxicol. Environ. Health Sci.* **2021**, *13*, 45–56. [[CrossRef](#)]
22. Gadade, J.P.; Patil, S.A. Phytochemical paradigm, antioxidant status and their correlation in *Rothea serrata* (L.) Steane and Mabb. *Ann. Phytomedicine Int. J.* **2019**, *8*, 156–166. [[CrossRef](#)]
23. Patel, J.J.; Acharya, S.R.; Acharya, N.S. *Clerodendrum serratum* (L.) Moon. A review on traditional uses, phytochemistry and pharmacological activities. *J. Ethnopharmacol.* **2014**, *154*, 268–285. [[CrossRef](#)]
24. Wang, J.H.; Luan, F.; He, X.D.; Wang, Y.; Li, M.X. Traditional uses and pharmacological properties of *Clerodendrum* phytochemicals. *J. Tradit. Complement. Med.* **2018**, *8*, 24–38. [[CrossRef](#)] [[PubMed](#)]
25. Kalonio, D.E.; Hendriani, R.; Barung, E.N. Anticancer activity of plant genus *Clerodendrum* (Lamiaceae): A Review. *Trad. Med. J.* **2017**, *22*, 182. [[CrossRef](#)]
26. Chakraborty, B.; Kumar, R.S.; Almansour, A.I.; Kotresha, D.; Rudrappa, M.; Pallavi, S.S.; Hiremath, H.; Perumal, K.; Nayaka, S. Evaluation of antioxidant, antimicrobial and antiproliferative activity of silver nanoparticles derived from *Galphimia glauca* leaf extract. *J. King Saud Univ. Sci.* **2021**, *33*, 101660. [[CrossRef](#)]
27. Chand, K.; Cao, D.; Eldin Fouad, D.; Hussain Shah, A.; Qadeer Dayo, A.; Zhu, K.; Nazim Lakhan, M.; Mehdi, G.; Dong, S. Green synthesis, characterization and photocatalytic application of silver nanoparticles synthesized by various plant extracts. *Arab. J. Chem.* **2020**, *13*, 8248–8261. [[CrossRef](#)]
28. Bhat, M.; Chakraborty, B.; Kumar, R.S.; Almansour, A.I.; Arumugam, N.; Kotresha, D.; Pallavi, S.S.; Dhanyakumara, S.B.; Shashiraj, K.N.; Nayaka, S. Biogenic synthesis, characterization and antimicrobial activity of *Ixora brachypoda* (DC) leaf extract mediated silver nanoparticles. *J. King Saud Univ. Sci.* **2021**, *33*, 101296. [[CrossRef](#)]
29. Kambale, E.K.; Nkanga, C.I.; Mutonkole, B.P.I.; Bapolisi, A.M.; Tassa, D.O.; Liesse, J.M.I.; Krause, R.W.M.; Memvanga, P.B. Green synthesis of antimicrobial silver nanoparticles using aqueous leaf extracts from three Congolese plant species (*Brillantaisia patula*, *Crossopteryx febrifuga* and *Senna siamea*). *Heliyon* **2020**, *6*, e04493. [[CrossRef](#)]
30. Ndikau, M.; Noah, N.M.; Andala, D.M.; Masika, E. Green synthesis and characterization of silver nanoparticles using *Citrullus lanatus* fruit rind extract. *Int. J. Anal. Chem.* **2017**, *62*, 3103–3105. [[CrossRef](#)] [[PubMed](#)]
31. Subba Rao, Y.; Kotakadi, V.S.; Prasad, T.N.V.K.V.; Reddy, A.V.; Sai Gopal, D.V.R. Green synthesis and spectral characterization of silver nanoparticles from Lakshmi tulasi (*Ocimum sanctum*) leaf extract. *Spectrochim. Acta Part A Mol. Biomol. Spectrosc.* **2013**, *103*, 156–159. [[CrossRef](#)]

32. Fard, N.N.; Noorbazargan, H.; Mirzaie, A.; Hedayati Ch, M.; Moghimiyani, Z.; Rahimi, A. Biogenic synthesis of AgNPs using *Artemisia oliveriana* extract and their biological activities for an effective treatment of lung cancer. *Artif. Cells Nanomed. Biotechnol.* **2018**, *46*, 1047–1058. [[CrossRef](#)]
33. Aritonang, H.F.; Koleangan, H.; Wuntu, A.D. Synthesis of silver nanoparticles using aqueous extract of medicinal plants (*Impatiens balsamina* and *Lantana camara*) fresh leaves and analysis of antimicrobial activity. *Int. J. Microbiol.* **2019**, *2019*, 8642303. [[CrossRef](#)]
34. Mussin, J.; Robles-Botero, V.; Casañas-Pimentel, R.; Rojas, F.; Angioletta, L.; San Martín-Martínez, E.; Giusiano, G. Antimicrobial and cytotoxic activity of green synthesis silver nanoparticles targeting skin and soft tissue infectious agents. *Sci. Rep.* **2021**, *11*, 14566. [[CrossRef](#)]
35. Mosmann, T. Rapid colorimetric assay for cellular growth and survival: Application to proliferation and cytotoxicity assays. *J. Immunol. Methods* **1983**, *65*, 55–63. [[CrossRef](#)] [[PubMed](#)]
36. Nagaraja, S.K.; Kumar, R.S.; Chakraborty, B.; Hiremath, H.; Almansour, A.I.; Perumal, K.; Gunagambhire, P.V.; Nayaka, S. Biomimetic synthesis of silver nanoparticles using *Cucumis sativus* var. *hardwickii* fruit extract and their characterizations, anticancer potential and apoptosis studies against Pa-1 (Human ovarian teratocarcinoma) cell line via flow cytometry. *Appl. Nanosci.* **2022**, *13*, 3073–3084. [[CrossRef](#)]
37. O'Brien, M.C.; Bolton, W.E. Comparison of cell viability probes compatible with fixation and permeabilization for combined surface and intracellular staining in flow cytometry. *Cytometry* **1995**, *19*, 243–255. [[CrossRef](#)]
38. Venkatesan, J.; Kim, S.-K.; Shim, M. Antimicrobial, antioxidant, and anticancer activities of biosynthesized silver nanoparticles using marine algae *Ecklonia cava*. *Nanomaterials* **2016**, *6*, 235. [[CrossRef](#)] [[PubMed](#)]
39. Zhang, X.-F.; Liu, Z.-G.; Shen, W.; Gurunathan, S. Silver nanoparticles: Synthesis, characterization, properties, applications, and therapeutic approaches. *Int. J. Mol. Sci.* **2016**, *17*, 1534. [[CrossRef](#)]
40. Lakshmanan, G.; Sathiyaseelan, A.; Kalaichelvan, P.T.; Murugesan, K. Plant-mediated synthesis of silver nanoparticles using fruit extract of *Cleome viscosa* L.: Assessment of their antibacterial and anticancer activity. *Karbala Int. J. Mod. Sci.* **2018**, *4*, 61–68. [[CrossRef](#)]
41. Rajesh Kumar, T.V.; Murthy, J.S.R.; Narayana Rao, M.; Bhargava, Y. Evaluation of silver nanoparticles synthetic potential of *Couroupita guianensis* Aubl., flower buds extract and their synergistic antibacterial activity. *3 Biotech* **2016**, *6*, 92. [[CrossRef](#)]
42. Al-Nuairi, A.G.; Mosa, K.A.; Mohammad, M.G.; El-Keblawy, A.; Soliman, S.; Alawadhi, H. Biosynthesis, characterization, and evaluation of the cytotoxic effects of biologically synthesized silver nanoparticles from *Cyperus conglomeratus* root extracts on breast cancer cell line MCF-7. *Biol. Trace. Elem. Res.* **2020**, *194*, 560–569. [[CrossRef](#)] [[PubMed](#)]
43. Algebaly, A.S.; Mohammed, A.E.; Abutaha, N.; Elobeid, M.M. Biogenic synthesis of silver nanoparticles: Antibacterial and cytotoxic potential. *Saud. J. Biol. Sci.* **2020**, *27*, 1340–1351. [[CrossRef](#)]
44. Chung, I.M.; Park, I.; Seung-Hyun, K.; Thiruvengadam, M.; Rajakumar, G. Plant-mediated synthesis of silver nanoparticles: Their characteristic properties and therapeutic applications. *Nanoscale Res. Lett.* **2016**, *11*, 40. [[CrossRef](#)]
45. Ajitha, B.; Reddy, Y.A.K.; Lee, Y.; Kim, M.J.; Ahn, C.W. Biomimetic synthesis of silver nanoparticles using *Syzygium aromaticum* (clove) extract: Catalytic and antimicrobial effects. *Appl. Organometal. Chem.* **2019**, *33*, e4867. [[CrossRef](#)]
46. Noorbazargan, H.; Amintehrani, S.; Dolatabadi, A.; Mashayekhi, A.; Khayam, N.; Moulavi, P.; Naghizadeh, M.; Mirzaie, A.; Mirzaei Rad, F.; Kavousi, M. Anti-cancer & anti-metastasis properties of bioorganic-capped silver nanoparticles fabricated from *Juniperus chinensis* extract against lung cancer cells. *AMB. Expr.* **2021**, *11*, 61. [[CrossRef](#)]
47. Arunachalam, K.; Annamalai, S.; Hari, S. One-step green synthesis and characterization of leaf extract-mediated biocompatible silver and gold nanoparticles from *Memecylon umbellatum*. *Int. J. Nanomed.* **2013**, *8*, 1307–1315. [[CrossRef](#)]
48. Goudarzi, M.; Mir, N.; Mousavi-Kamazani, M.; Bagheri, S.; Salavati-Niasari, M. Biosynthesis and characterization of silver nanoparticles prepared from two novel natural precursors by facile thermal decomposition methods. *Sci. Rep.* **2016**, *6*, 32539. [[CrossRef](#)] [[PubMed](#)]
49. Donga, S.; Chanda, S. Facile green synthesis of silver nanoparticles using *Mangifera indica* seed aqueous extract and its antimicrobial, antioxidant and cytotoxic potential (3-in-1 system). *Artif. Cells Nanomed. Biotechnol.* **2021**, *49*, 292–302. [[CrossRef](#)] [[PubMed](#)]
50. Ardestani, M.S.; Sadat Shandiz, S.A.; Salehi, S.; Ghanbar, F.; Darvish, M.R.; Mirzaie, A.; Jafari, M. Phytosynthesis of silver nanoparticles using *Artemisia marschalliana* Sprengel aerial part extract and assessment of their antioxidant, anticancer, and antibacterial properties. *Int. J. Nanomed.* **2016**, *11*, 1835. [[CrossRef](#)]
51. Chandraker, S.K.; Ghosh, M.K.; Lal, M.; Shukla, R. A review on plant-mediated synthesis of silver nanoparticles, their characterization and applications. *Nano Express* **2021**, *2*, 022008. [[CrossRef](#)]
52. Ajitha, B.; Ashok Kumar Reddy, Y.; Sreedhara Reddy, P. Green synthesis and characterization of silver nanoparticles using *Lantana camara* leaf extract. *Mater. Sci. Eng.* **2015**, *49*, 373–381. [[CrossRef](#)]
53. El-Aswar, E.I.; Zahran, M.M.; El-Kemary, M. Optical and electrochemical studies of silver nanoparticles biosynthesized by *Haplophyllum tuberculatum* extract and their antibacterial activity in wastewater treatment. *Mater. Res. Express* **2019**, *6*, 105016. [[CrossRef](#)]
54. Moteriya, P.; Chanda, S. Synthesis and characterization of silver nanoparticles using *Caesalpinia pulcherrima* flower extract and assessment of their in vitro antimicrobial, antioxidant, cytotoxic, and genotoxic activities. *Artif. Cells Nanomed. Biotechnol.* **2017**, *45*, 1556–1567. [[CrossRef](#)] [[PubMed](#)]

55. Sun, Q.; Cai, X.; Li, J.; Zheng, M.; Chen, Z.; Yu, C.P. Green synthesis of silver nanoparticles using tea leaf extract and evaluation of their stability and antibacterial activity. *Colloids Surf. A Physicochem. Eng. Asp.* **2014**, *444*, 226–231. [[CrossRef](#)]
56. Heidari, Z.; Salehzadeh, A.; Sadat Shandiz, S.A.; Tajdoost, S. Anti-cancer and anti-oxidant properties of ethanolic leaf extract of *Thymus vulgaris* and its bio-functionalized silver nanoparticles. *3 Biotech* **2018**, *8*, 177. [[CrossRef](#)] [[PubMed](#)]
57. Mata, R.; Nakkala, J.R.; Sadras, S.R. Biogenic silver nanoparticles from *Abutilon indicum*: Their antioxidant, antibacterial and cytotoxic effects in vitro. *Colloids Surf. B Biointerfaces* **2015**, *128*, 276–286. [[CrossRef](#)]
58. Balan, K.; Qing, W.; Wang, Y.; Liu, X.; Palvannan, T.; Wang, Y.; Ma, F.; Zhang, Y. Antidiabetic activity of silver nanoparticles from green synthesis using *Lonicera japonica* leaf extract. *RSC Adv.* **2016**, *6*, 40162–40168. [[CrossRef](#)]
59. Sriranjani, R.; Srinithya, B.; Vellingiri, V.; Brindha, P.; Anthony, S.P.; Sivasubramanian, A.; Muthuraman, M.S. Silver nanoparticle synthesis using *Clerodendrum phlomidis* leaf extract and preliminary investigation of its antioxidant and anticancer activities. *J. Mol. Liq.* **2016**, *220*, 926–930. [[CrossRef](#)]
60. Ravichandran, V.; Vasanthi, S.; Shalini, S.; Ali Shah, S.A.; Harish, R. Green synthesis of silver nanoparticles using *Atrocarpus altilis* leaf extract and the study of their antimicrobial and antioxidant activity. *Mater. Lett.* **2016**, *180*, 264–267. [[CrossRef](#)]
61. Kokila, T.; Ramesh, P.S.; Geetha, D. Biosynthesis of AgNPs using *Carica Papaya* peel extract and evaluation of its antioxidant and antimicrobial activities. *Ecotoxicol. Environ. Saf.* **2016**, *134*, 467–473. [[CrossRef](#)]
62. Kim, J.S.; Kuk, E.; Yu, K.N.; Kim, J.H.; Park, S.J.; Lee, H.J.; Kim, S.H.; Park, Y.K.; Park, Y.H.; Hwang, C.Y.; et al. Antimicrobial effects of silver nanoparticles. *Nanomed. Nanotechnol. Biol. Med.* **2007**, *3*, 95–101. [[CrossRef](#)]
63. Rajeshkumar, S.; Malarkodi, C.; Vanaja, M.; Annadurai, G. Anticancer and enhanced antimicrobial activity of biosynthesized silver nanoparticles against clinical pathogens. *J. Mol. Struct.* **2016**, *1116*, 165–173. [[CrossRef](#)]
64. Khan, I.; Saeed, K.; Khan, I. Nanoparticles: Properties, applications and toxicities. *Arab. J. Chem.* **2019**, *12*, 908–931. [[CrossRef](#)]
65. Saratale, G.D.; Saratale, R.G.; Benelli, G.; Kumar, G.; Pugazhendhi, A.; Kim, D.S.; Shin, H.S. Anti-diabetic potential of silver nanoparticles synthesized with *Argyrea nervosa* leaf extract high synergistic antibacterial activity with standard antibiotics against foodborne bacteria. *J. Clust. Sci.* **2017**, *28*, 1709–1727. [[CrossRef](#)]
66. Lee, Y.J.; Song, K.; Cha, S.H.; Cho, S.; Kim, Y.S.; Park, Y. Sesquiterpenoids from *Tussilago farfara* flower bud extract for the eco-friendly synthesis of silver and gold nanoparticles possessing antibacterial and anticancer activities. *Nanomaterials* **2019**, *9*, 819. [[CrossRef](#)]
67. Qais, F.A.; Shafiq, A.; Khan, H.M.; Husain, F.M.; Khan, R.A.; Alenazi, B.; Alsalmeh, A.; Ahmad, I. Antibacterial effect of silver nanoparticles synthesized using *Murraya Koenigii* (L.) against multidrug-resistant pathogens. *Bioinorg. Chem. Appl.* **2019**, *2019*, 4649506. [[CrossRef](#)] [[PubMed](#)]
68. Jalal, M.; Ansari, M.; Alzohairy, M.; Ali, S.; Khan, H.; Almatroudi, A.; Raees, K. Biosynthesis of silver nanoparticles from Oropharyngeal *Candida glabrata* isolates and their antimicrobial activity against clinical strains of bacteria and fungi. *Nanomaterials* **2018**, *8*, 586. [[CrossRef](#)] [[PubMed](#)]
69. Kanniah, P.; Chelliah, P.; Thangapandi, J.R.; Gnanadhas, G.; Mahendran, V.; Robert, M. Green synthesis of antibacterial and cytotoxic silver nanoparticles by *Piper nigrum* seed extract and development of antibacterial silver based chitosan nanocomposite. *Int. J. Biol. Macromol.* **2021**, *189*, 18–33. [[CrossRef](#)] [[PubMed](#)]
70. Nagaraja, S.K.; Niazi, S.K.; Bepari, A.; Assiri, R.A.; Nayaka, S. *Leonotis nepetifolia* flower bud extract mediated green synthesis of silver nanoparticles, Their characterization, and In vitro evaluation of biological applications. *Materials* **2022**, *15*, 8990. [[CrossRef](#)] [[PubMed](#)]

Disclaimer/Publisher’s Note: The statements, opinions and data contained in all publications are solely those of the individual author(s) and contributor(s) and not of MDPI and/or the editor(s). MDPI and/or the editor(s) disclaim responsibility for any injury to people or property resulting from any ideas, methods, instructions or products referred to in the content.